Influence of Permeability on Sediment Trapping Efficiency in an ELJ Groyne Field

J. A. Bautista[1]; J. M. Kuroiwa, Ph.D., P.E., A.M.ASCE[2]; J. F. Huamán, Ph.D., P.E.[3]; and L. F. Castro[4]

[1]Graduate Student, Universidad Nacional de Ingeniería, Lima, Perú; Formerly Student at Universidad Nacional de Cajamarca, Perú. E-mail: jabautistam@unc.edu.pe
[2]Director, National Hydraulics Laboratory and Professor, School of Civil Engineering, Universidad Nacional de Ingeniería, Av. Túpac Amaru Nº 210, Rímac, Apartado 1301, Perú. E-mail: jkuroiwa@uni.edu.pe
[3]Professor, Universidad Nacional de Cajamarca, Cajamarca, Perú. E-mail: jfranhvid@yahoo.es
[4]Instructor and Researcher, National Hydraulics Laboratory, Universidad Nacional de Ingeniería, Av. Túpac Amaru Nº 210, Rímac, Apartado 1301, Peru. E-mail: lfcastro@uni.edu.pe

ABSTRACT

In woody areas where traditional construction materials are not available engineered log jams (ELJ) may constitute a potential solution for controlling riverbank erosion. Two ELJ groyne fields formed by four structures were placed in a 12 m long rectangular flume. In the first setup, groynes had a 46% permeability whereas in the second setup, groynes had a 26% permeability. Sediment in suspension was incorporated at a constant rate after flow was stabilized. Tests showed that when groyne permeability has higher, maximum scour depth at the inner end of the groyne diminished while sediment deposition between groynes increased. This result indicates that use of the main resource for building ELJ groynes can be optimized. As the configuration of the groynes was basically idealized as a frame of cylindrical elements, results of this experimental program may also be used to design groynes made up of artificial materials resembling ELJs. This type of solution could be used where traditional construction materials are not readily available.

INTRODUCTION

The Amazon Jungle lacks sources of construction material. For instance, rock and gravel can not be found within the lowlands of the Amazon Jungle. However, arboreous vegetation is abundant and can even been found near riverbanks and floating on watercourses. There are a number of researchers who have studied different methods to control bank erosion.

Spurs (groynes) and retards are used to slow flow near the banks and deflect flows towards the center of the watercourse. They can be permeable or impermeable and can be built of different materials, including timber (Richardson et al 2001). Wood has been used to build dykes, retards and other fluvial and marine structures to control erosion for centuries. Engineered Log Jams (ELJ), in its modern form, have been successfully used in small streams in Scotland and in the United States of America. Habitat was noticeably improved after this measure was implemented mainly to control erosion (Herrera Environmental Consultants 2006). Shields et al (2004) indicate that Large Woody Debris Structures (LWDS) could be a low-cost solution to rehabilitate small streams whose drainage area is under 200 km^2. Success implies controlling erosion and the recovery of the ecosystem. These structures are vulnerable if not enough sediments deposit within their interstices to counteract flotation forces. Wood decomposition before sediments have deposited in sufficient volume between ELJs and enough vegetation has been stablished to provide adequate stability to the structure may also pose a problem. Yossef

and de Vriend (2010) studied sediment exchange between the main channel and the groyne field formed by impermeable structures and concluded that there is a net import of sediment into the groyne field. In addition, prevailing transport mechanisms vary with flow depth. If the structures are unsubmerged, advection by the primary circulation cell controls sediment transport. If they are submerged, residual advection by large-scale coherent flow controls sediment transport. Cao et al (2013) indicate that optimal permeability of a groyne depends upon a number of parameters such as flow velocity, local turbulence, gran size distribution and is strongly related to structural conditions and geometry of the groyne field. By increasing groyne permeability, flow separation effects are reduced as well as the formation of large eddies and return currents. These phenomena intensify scour near the inner end of the groyne.

Literature review suggested that differences in sediment deposition in the groyne field as well as scour near the tip of a groyne occur due to the difference of permeability in this type of structures. Therefore, an experimental study was conducted by Bautista (2018) to study the effect of permeability on scour and deposition patterns in a groyne field. This paper summarizes the results of his investigation. Recommendations given in Yalin (1972), ASCE (2000), Aberle et al (2017), Muste et al (2017) and Gallisdorfer et al (2014) were taken into account for designing the experiments.

DESCRIPTION OF FACILITIES AND EQUIPMENT

Tests were conducted at the Didactic Division, an indoors facility of the National Hydraulics Laboratory (LNH, acronym in Spanish). This research center is located at the National University of Engineering campus in Lima, Perú.

Four sump pumps with a nominal maximum capacity of 700 L/s have been installed at the LNH. They can pump water from an 80 m^3 underground reservoir, located underneath the Didactic Division building, to an elevated concrete reservoir whose capacity is 5 m^3. This structure is located 5 m above ground level. One of the pumps, whose nominal discharge is 200 L/s and nominal power is 37.29 Kw (50 HP), was used to carry out the tests. Flow was controlled by a 356 mm slide gate and a by-pass valve. One 356 mm internal diameter pipe delivered water to the inlet of the experimental module. An upstream stilling basin reduced water turbulence. Water passed through hollow bricks located near the bottom of the stilling basin entering a second stilling basin where a rectangular weir allowed discharge measurement. A Neyrpic hook gauge installed outside the stilling basin measured water levels in a cylindrical connected to the stilling basin with a transparent hose. This device allowed water level measurement that was correlated with incoming discharge. Downstream of the weir a metal mesh reduced turbulence generated by impact in a third stilling basin. Water entered the flume by overflow from a rectangular reservoir. Water passed again through hollow bricks that straightened the flow before entering the rectangular reservoir.

The testing section of the flume was 12 m long, 1.9 m wide and the groyne length, perpendicular to the flume was 0.475 m, this is, one fourth of the internal width of the flume. Total height was 1.4 m and allowed to place a 1 m thick bed and 0.4 m for flow depth and freeboard. Acrylic glass (Polymethyl methacrylate or PMMA) windows allowed visualization of both scour progression in time and flow patterns in the vicinity of the groynes. Four ELJ groynes were installed on the right side of the flume (looking downstream). Spacing between these structures was 2 m. At the downstream end, a rectangular tilting gate is used to control water levels. A schematic of the experiment setup is shown in Figure 1.

Two types of Engineered Log Jams groynes were tested. Cylindrical wood pieces with a

short and wider cylindrical cross section at the bottom simulated logs. Groyne permeability was changed by modifying spacing between main and secondary frame elements. Permeability is defined as the void area to total projected area ratio as defined by Mahmoud Mustafa et al (2012). In the 26% permeability groyne void area and projected groyne area were 275 cm^2 and 1058 cm^2, respectively. In the second case, void area and projected groyne area were 486.6 cm^2 and 1058 cm^2, respectively, rendering a 46% permeability.

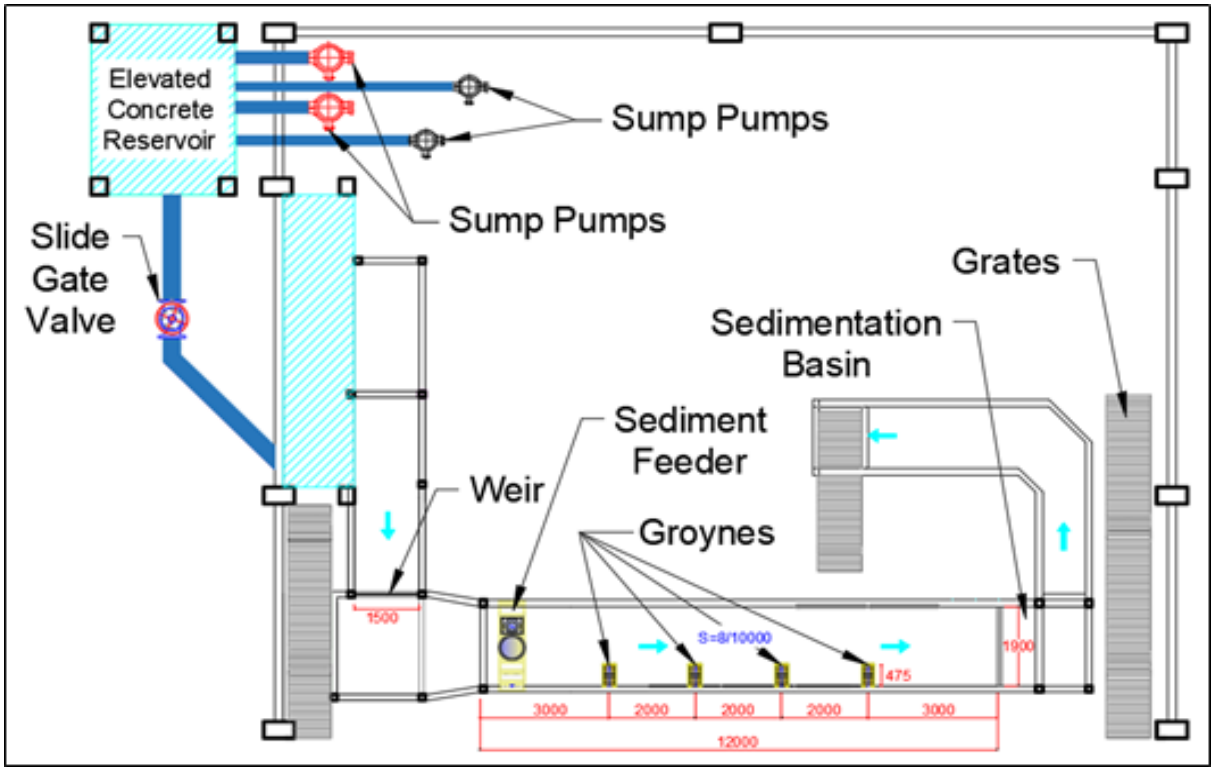

Figure 1. Schematic of experimental setup. Dimensions are shown in millimeters.

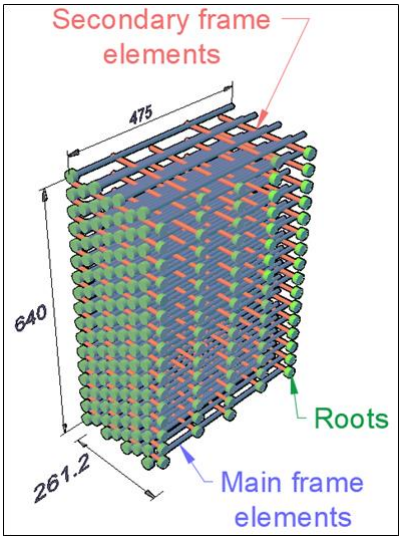

Figure 2. Schematic of groyne element. Dimensions are given in millimeters.

A mason leveled the bed with the aid of a wooden plank, checking bed levels every 500 mm.

Slope was held constant at 0.0008. Bed material was composed by sand whose median diameter (d_{50}), d_{80}, and standard deviation were 0.204 mm, 0.4 mm and 1.61 mm, respectively. Critical shear stress was much lower than acting shear stress for the bed material. Median diameter (d_{50}) of the sediment in suspension was 0.175 mm whereas d_{80} and the standard deviation where 0.287 mm and 1.61, respectively. Sediment size distribution was chosen so that suspension of sediments would occur along a water column. Suspension number was 1.87 for the bed material and 1.326 for the sediments fed into the flume. Considerations exposed in Van Rijn (1993) were taken into account.

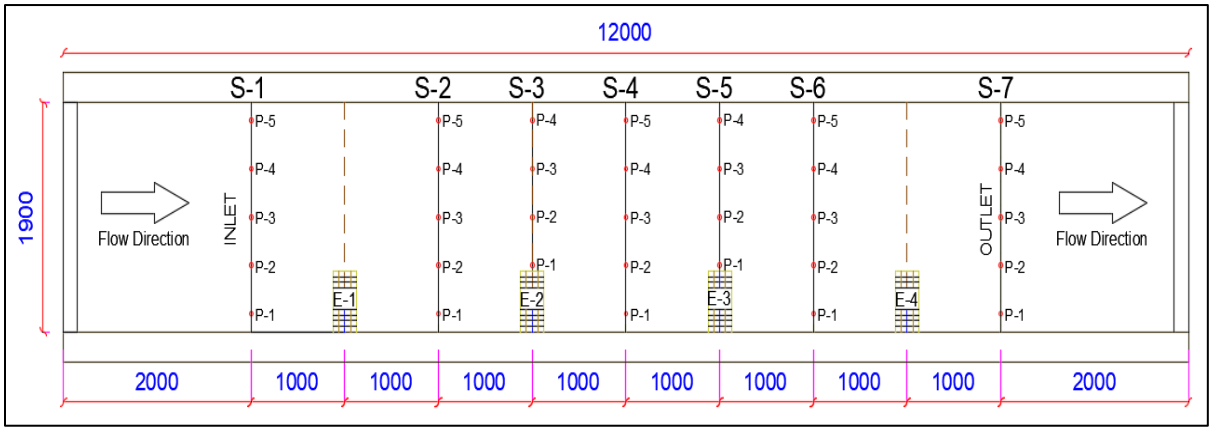

Figure 3. Schematics of testing area showing cross sections where velocity field data and sediments were collected. Dimensions are shown in millimeters.

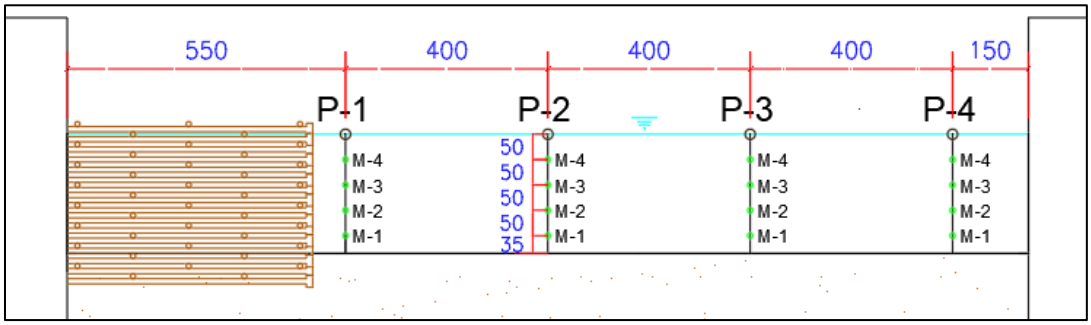

Figure 4. Locations where sediment samples were taken in Sections S-3 and S-5.

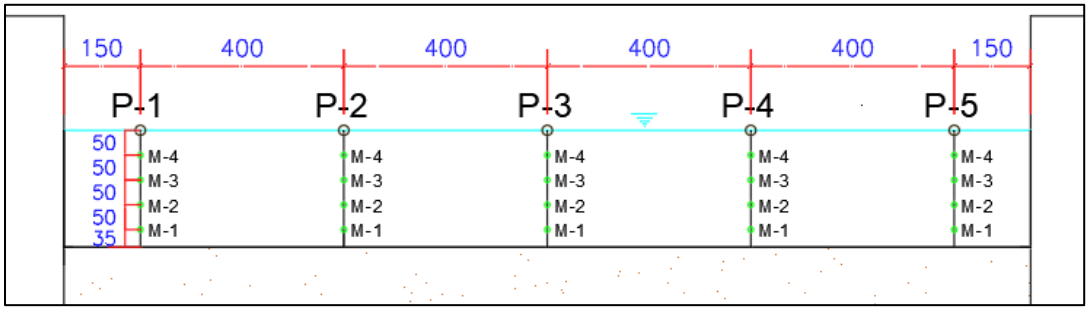

Figure 5. Locations where sediment samples were taken in Sections S-1, S-2, S-4, S-6 and S-7.

Sediment was incorporated by using a Syntron type sediment feeder. A moving steel platform that ran on rails mounted on the flume walls was used to provide support to the

personnel in charge of tests and the instruments, namely, the Acoustic Doppler Velocimeter Profiler (ADV Profiler), the limnimeter and the suspended sediment collection equipment. The latter consisted of five 9.53 mm diameter plastic tubes that collected sediment by syphoning into labeled glass beakers. Spacing between sediment collecting tubes was 50 mm. The mixture of water and sediment was weighted in a precision electronic scale and dried using an electric oven and dried sediments were weighted again. Temperature of the water was measured with an electronic thermometer whose precision was 0.1°C.

A 3D scanner allowed scanning of the bed with a 2 mm precision. This device could scan up to a distance of 120 m with an angle of 360º around a horizontal axis and 305º on a vertical axis. It could also take highly realistic photographs creating files of up to 70 Megapixels.

TESTING PROCEDURES AND DATA ACQUISITION

The flume bed was leveled the day before each test was conducted. Valves were slowly opened to fill the flume with water without producing scour. Level was held constant with the aid of the rectangular tilting gate, located at the downstream end of the flume.

Figure 6. Test conditions during the 46% permeability tests. Polystyrene balls were added for visualizing the flow field.

Once the target level was reached, the slide gate valve was slowly opened to increase discharge and proper gate adjustments were made. Discharge was monitored at the rectangular

weir. A previously stablished hydrograph was applied until the target discharge was attained.

Tests did not start until the testing section reached the target discharge and the target water level was kept constant for more than 30 minutes. After flow and water levels were stable, the sediment feeder was started and the sediment/water mix was incorporated into the main flow. Velocity fields were recorded using the ADV profiler. This device collects velocity data in the three directions and obtain velocity profiles in discrete cells. Data was stored and analyzed in a i7 laptop computer loaded with the ADV controller and Paraview. This open-source computer program was used for velocity analysis and obtaining cross sections.

Sediments in suspension and velocity fields were collected at designated points as shown in Figures 3, 4 and 5. P-1 trough P-5 were the vertical lines where velocity fields and sediment samples were collected in sections S-1, S-2, S-4, S-6 and S-7. In sections S-3 and S-5 vertical alignments used were P-1 through P-4. Locations M-1 to M-4 show the positions were sediment samples were collected. In each position a graduated cylinder with a 1000 ml capacity was filled. Water with sediments was weighted and it was dried at 110º C in an electric oven for four hours. Dry sediments were weighted again to obtain the dry weight and sediment concentration was calculated. Sediment transport was estimated at each cross section integrating sediment concentration and velocities in the vertical direction.

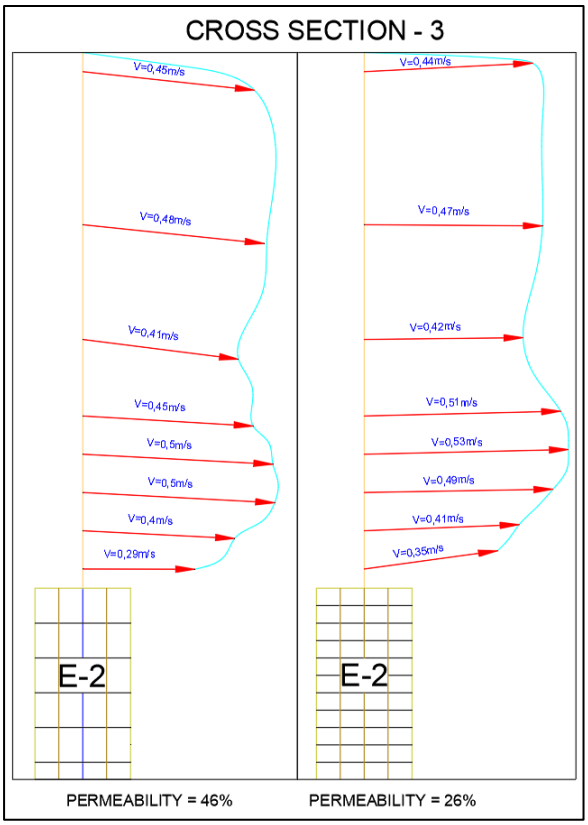

Figure 7. Velocity fields in the 46% and 26% permeability tests at cross section S-3.

RESULTS AND DISCUSSION

Velocity fields were processed to obtain velocities at different, discrete points along the vertical axis. Average velocity of the flow in both tests was 0.334 m/s while the depth was approximately 0.245 m, rendering a Fr = 0.22. Therefore, flow was subcritical throughout the

tests. Figure 6 shows flow conditions during the 46% permeability tests.

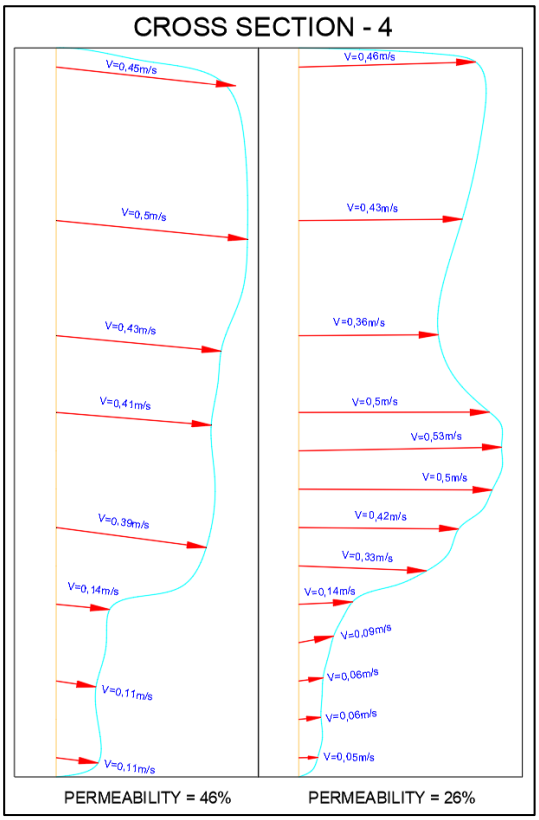

Figure 8. Velocity files in the 46% and 26% permeability tests at cross section S-4.

Velocity fields were altered by the presence of the groyne field. Flow deviation towards the center of the flume was more pronounced in the lower permeability setup. Although absolute values of the velocities were not very different in both tests, velocity vectors near the inner, upstream end of the groyne showed significant deviation towards the center of the flume in the lower permeability test as shown in Figure 6. Figure 7 shows that at cross section 4, immediately downstream of the second groyne (E-2), velocities are slightly higher in the 46% permeability test near the right wall allowing sediments to pass through E-2. It is also shown that the velocity field points towards the wall. Lower velocities in the direction of the wall may favor deposition of the sediments in between groynes. Flow direction change is more pronounced near the inner end of the groyne in the 26% permeability tests. This induces more erosion at the base of the structures and also pushes sediments towards the interior of the flume. This can explain, in part, why deposition in between groynes is greater in the 46% permeability tests.

Figure 9 presents velocities averaged in the vertical in cross section P-5 in both tests. Notice that the less permeable structure diverts flow and sediments towards the left bank whereas the more permeable structure diverts water to the right bank, where greater deposition occurs.

Concentration profiles and velocity profiles were obtained after data were processed. Figures 10 and 11 show concentration profile at section S-1 and velocity profile at Section S-1, respectively. Concentration was greater near the bed and decreased upwards in all cross sections were sediments were collected.

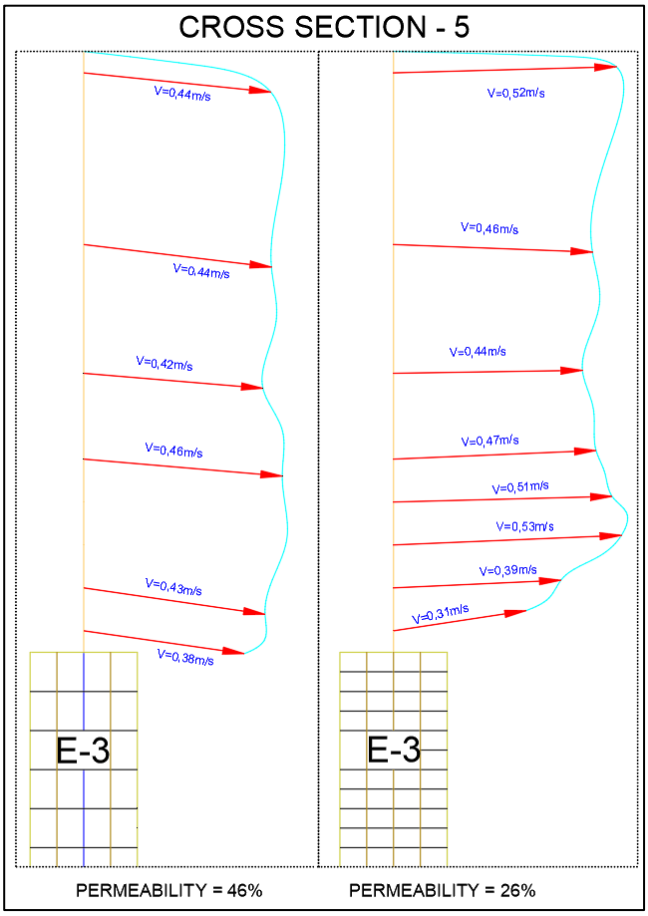

Figure 9. Velocity fields in the 46% permeability and 26% permeability tests. Notice the change in flow direction near the inner end of the groyne.

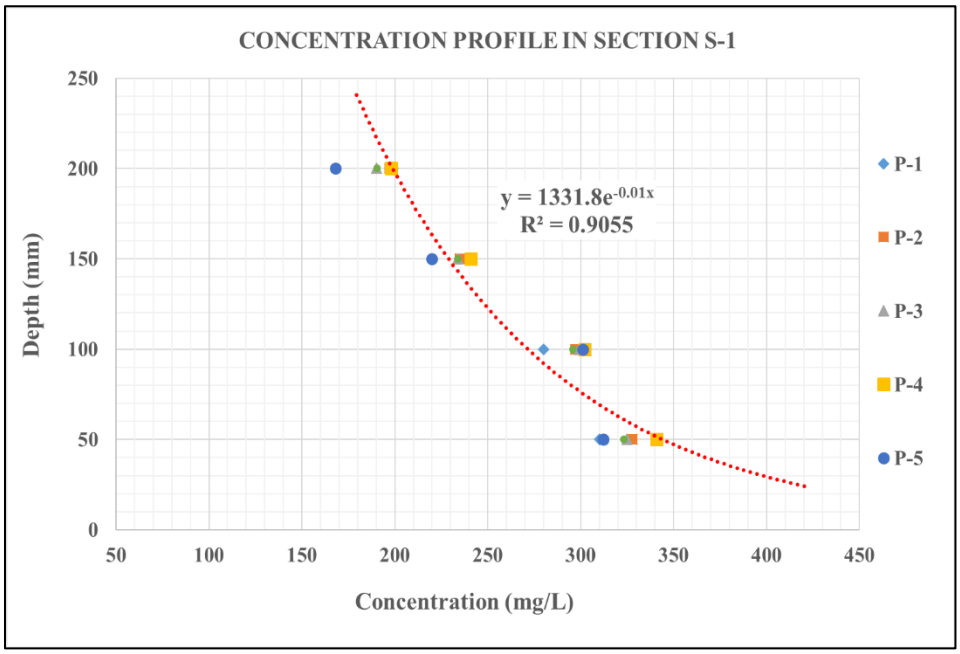

Figure 10. Concentration profile in Section S-1 for test at 46% permeability.

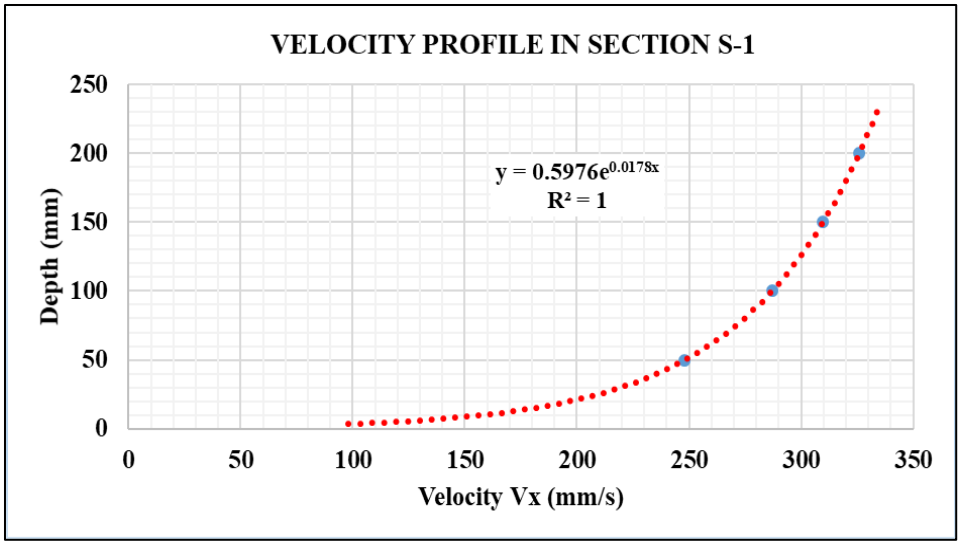

Figure 11. Velocity profile in Section S-1 for test at 46% permeability.

Figure 12. Scour and deposition patterns and bedforms after the 26% permeability test was concluded.

Three-dimensional scanning of the bed showed bed elevation changes in the test area. Lower

permeability of the groynes increased maximum local scour near their inner ends whereas deposition was lower between groynes. Figures 12 and 13 shows the bed after the 26% and 46% permeability tests, respectively, were concluded and the flume was drained. It was observed that the predominant bedform was dunes. Scour and deposition patterns could be easily identified. Figure 14 shows bed topography after 3D scan data was processed. Figure 15 includes flume walls and inlet and outlet structures besides the flume bed. Cross sections were obtained using Paraview, an open-source, multi-platform software for data analysis and visualization application. It was also used for obtaining average velocities integrated along vertical axes.

Figure 13. Scour and deposition patterns and bedforms after the 46% permeability test was concluded.

Sediment transport capacity was diminished by the presence of the groyne field. However, this effect was more pronounced in the higher permeability groyne field. Therefore, deposition was greater in the higher permeability tests. Calculations showed that sediment transport rate was 2.51 kg/min in the inlet and 1.73 kg/min in the outlet in the 26% permeability test. Estimated rate of deposition was 0.78 Kg/min. In the 46% permeability tests the inlet sediment transport rate was 1.92 Kg/min and 1.07 Kg/min in the outlet. In this case the estimated rate of deposition was 0.85 Kg/min. Gross sediment retention was 408 kg in the 46% permeability tests and 374.4 kg in the 26% permeability tests.

Figure 16, shows that in the greater permeability tests, final bed levels were greater that the initial bed levels in section S-4, between groynes E-2 and E-3. In the 26% permeability tests some scour occurred downstream of E-2. Bed changes at other cross sections are shown in Appendix A, at the end of this paper.

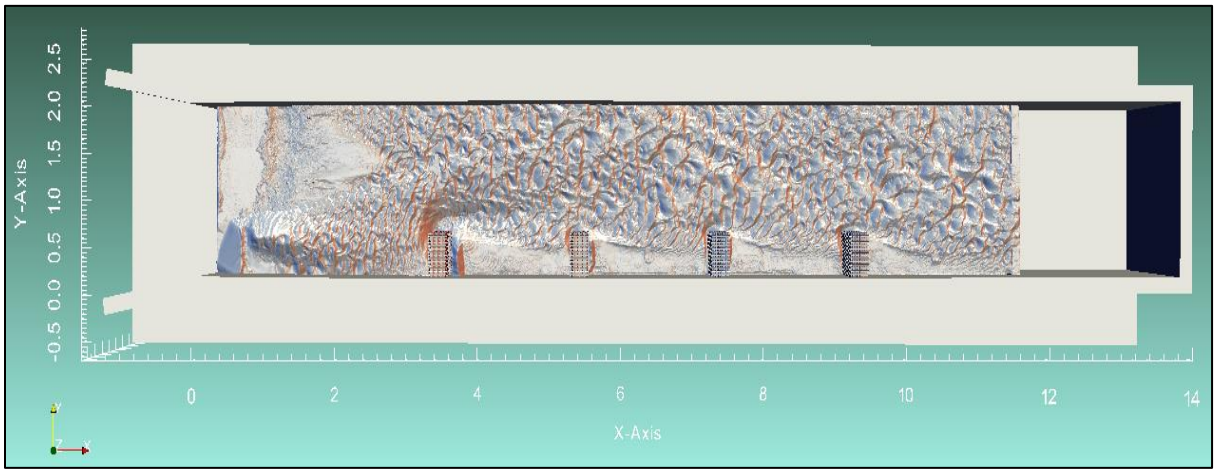

Figure 14: 3D scanning of the bed for 26% of permeability test

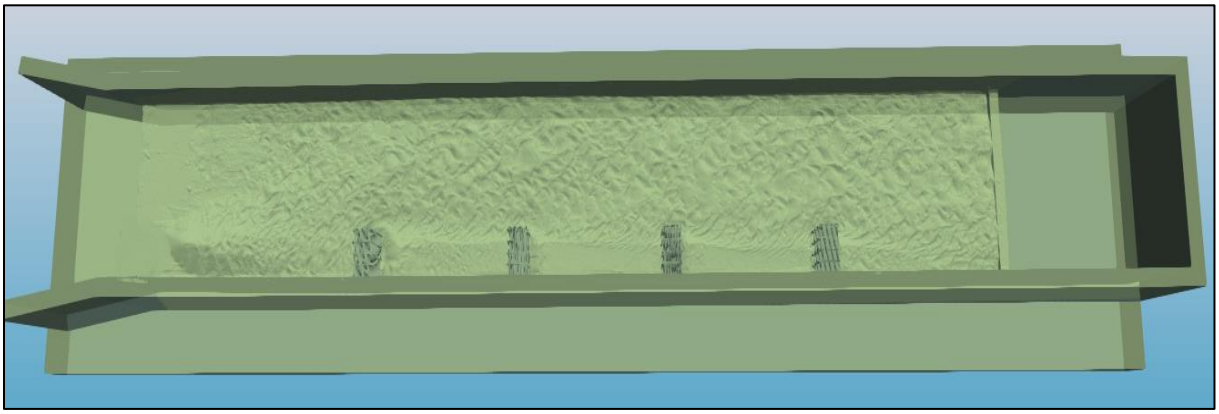

Figure 15. Tridimensional view of the inlet, testing and outlet section of the flume.

Table 1 includes maximum scour depth and maximum height of deposition in cross sections S-1 through S-7. It can be clearly seen that, within the groyne field, deposition is greater in the 46% permeability tests as deposition depth is greater in almost all cases, but particularly in between groynes. Scour depth is greater in the 26% permeability tests. One exception is in cross section S-3 where scour is greater in the 46% permeability tests by only 3 mm.

Results presented in this article indicate that it may be possible to protect river banks with a more permeable, and therefore, more efficient ELJ structure by diminishing the amount of material used in its construction.

CONCLUSIONS AND RECOMMENDATIONS

Conclusions

An experimental program was conducted to study the sediment trapping efficiency of two groyne field formed by four structures in which the varying factor was groyne permeability. In

the first case, permeability was 26% and in the second one was 46%.

After tests were conducted, velocity and sediment data were analyzed and suspended sediment transport was estimated between the inlet and the outlet of the experimental reach. Scour and deposition was estimated between groyne elements. Bed topography was obtained by 3D scanning.

Figure 16. Final bed levels in cross section S-4. Notice that bed levels in the 46% permeability test was greater than in the 26% permeability test. Dimensions are shown in millimeters.

After data was analyzed the following conclusions were derived from the experimental study:

- Direction of velocity changes more drastically in the less permeable groynes near the inner end. This causes a greater depth of scour. Therefore, maximum scour depth near the inner end of the ELJ groyne diminishes when permeability increases.
- Sediment deposition was greater in the groyne field with the greater permeability. Streamlines in the higher permeability tests show that velocities have a traverse component that directs flow and sediments toward the flume walls.

Table 1. Maximum scour depth and deposition heights in cross sections S-1 through S-7.

Cross Section	Permeability = 26%		Permeability = 46%	
	Maximum Scour Depth (mm)	Maximum Deposition Height (mm)	Maximum Scour Depth (mm)	Maximum Deposition Height (mm)
S-1	22.9	101.4	5.5	104.2
S-2	53.5	45.8	0	73
S-3	32.8	47.8	36.4	74.6
S-4	13.7	48.0	0	50.8
S-5	52.5	56.4	14	39.3
S-6	42.7	30.5	16.5	45.5
S-7	14.0	40.0	20.0	50.0

Results of this experiment could also be used in groynes of similar geometries regardless of constituting materials. For instance, large frames may also be made up of metal alloys in places where traditional construction materials may not be available.

Recommendations

Further tests need to be conducted to find the optimal combination of permeability, groyne relative length and angle of inclination with respect to the flow that allows greater sediment deposition in a groyne field and reduces maximum local scour near the inner end of the ELJ structures. Permeability, angle of inclination with respect to the flow and length of the groynes should vary to increase the experiments´ database. In addition, control of incoming sediment should also be improved when conducting this type of experiment for better comparison between runs.

ACKNOWLEDGMENTS

This study was partially funded through contract Nº 358-PNICP-PIAP-2014 between the National University of Engineering (UNI) and the National Innovation Program for Competitiveness and Productivity of the Ministry of Production (INNOVATE PERU).

The authors would like to thank Alfredo Jacay, Walter Chuan, Junior Galarza, Mishel Reyes, Jhostyn Nina, Walter Asalde, and Deivi Huaraca who assisted the first author during the experimental phase of the project.

REFERENCES

ASCE, (2000). *Hydraulic Modeling: Concepts and Practice. First Edition*. ASCE Press. Virginia, USA.

Aberle, J., Rennie, C., Admiraal, D., & Muste, M. (2017). *Experimental Hydraulics: Methods, Instrumentation, Data Processing and Management. Volume II: Instrumentation and Measurement Techniques. Third Edition*. Editorial CRC Press/Balkema. Leiden, The Netherlands.

Bautista, Jhon Alex (2018). *Eficiencia De Un Sistema De Espigones Permeables Fabricados Con Troncos De Árboles En La Retención De Sedimentos En Ríos Amazónicos* (In Spanish). Thesis for obtaining the Hydraulic Engineer Professional Title. Universidad Nacional de Cajamarca. Cajamarca, Peru.

Bennett, S.J.; Mohammad Ghaneeizad, S.; Gallisdorfer, M.; Donghua Cai; Atkinson, J.; Simon, A. & Langendoen, E. (2015). "Flow, Turbulence, And Drag Associated with Engineered Log Jams in A Fixed-Bed Experimental Channel". Geomorphology 248 (2015) 172–184

Cao, Y., Liu, P., & Jiang, E. (2013). *The Design and Application of Permeable Groynes*. Li Tian and Hetao Hou Editorial. Beijing, China.

Gallisdorfer, M., Bennett, S., Atkinson, J., Mohammad Ghaneeizad, S., Brooks, A., Simon, A., & Langendoen, E. (2014). "Physical-scale model designs for engineered log jams in rivers." Journal of Hydro-environment Research (8) 115-128.

Herrera Environmental Consultants (2006). *Application of Engineered Logjams - Conceptual Design Guidelines*. Scottish Environmental Protection Agency. Scotland, UK

Mahmoud M.M., Ahmed; H.S., Abd El-Raheem G.A.; Ali N.A. and Tominaga A. (2013). "Flow analysis around groyne with different permeability in compound channel floodplains." Journal of engineering sciences 41(2):302-320

Yossef, M.F.M. & de Vriend H.J (2010) "Sediment Exchange between a River and its Groyne Fields: Mobile-Bed Experiment". *J. Hydraul. Eng.* 136(9): 610-625.
Yossef, Mohamed F.M. (2002). *The Effect of Groynes on Rivers. Literature Review.* Delft University of Technology. Delft, The Netherlands.
Muste, M., Lyn, D., Admiraal, D., Ettema, R., Nikora, V., & Garcia, M. (2017). *Experimental Hydraulics: Methods, Instrumentation, Data Processing and Management. Volume I: Fundamentals and Methods*. CRC Press/Balkema. Leiden, The Netherlands.
Richardson, E.V.; Simons, D.B. and Lagasse P.F. (2001). *River Engineering for Highway Encroachments*. Report No. FHWA NHI 01-004 HDS 6. Federal Highway Administration. Washington DC, USA.
Shields, F.; Morin, N. & Cooper, C.M. (2004) "Large Woody Debris Structures for Sand-Bed Channels". *J. Hydraul. Eng.*, 130 (3) 208-217.
Van Rijn, L. C. (1993). *Principles of Sediment Transport in Rivers, Estuaries and Coastal Seas. First Edition*. Aqua Publications. Amsterdam, The Netherlands.
Yalin, M. S. (1972). *Mechanics of Sediment Transport. First Edition*. Pergamon Press. New York, USA.

APPENDIX A. BED CHANGES AT DIFFERENT CROSS SECTIONS

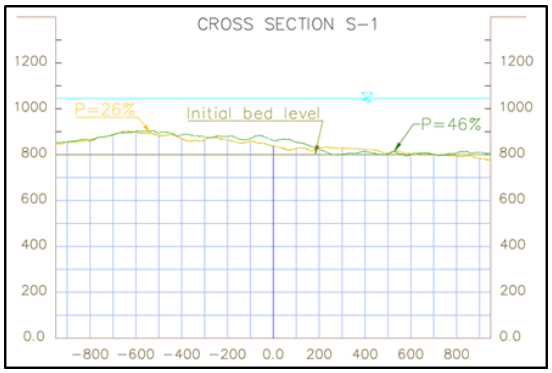

Figure 17. Bed changes at S-1 for the 26 and 46% permeabilities.

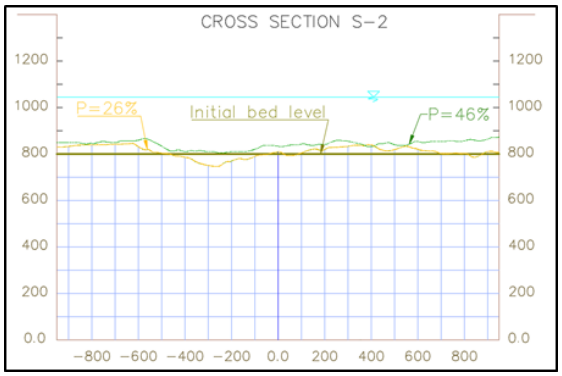

Figure 18. Bed changes at S-2 for the 26 and 46% permeabilities.

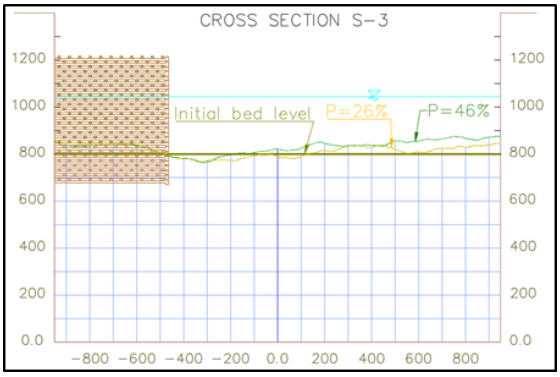

Figure 19. Bed changes at S-3 for the 26 and 46% permeabilities.

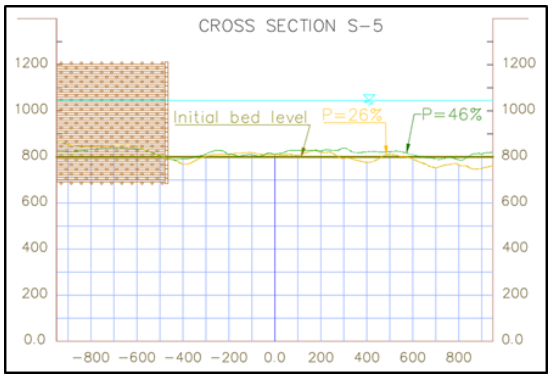

Figure 20. Bed changes at S-5 for the 26 and 46% permeabilities.

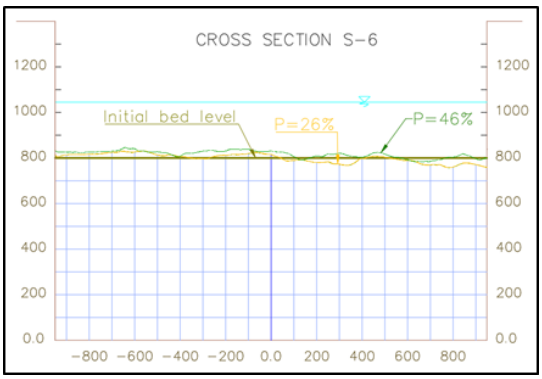

Figure 21. Bed changes at S-6 for the 26 and 46% permeabilities.

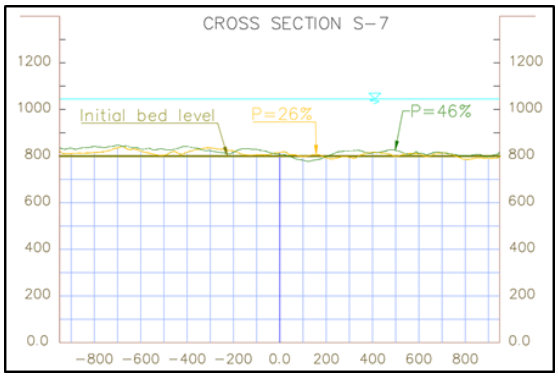

Figure 22. Bed changes at S-7 for the 26 and 46% permeabilities.